Reconstruction of the Holocene seismotectonic activity of the Southern Andes from seismites recorded in Lago Icalma, Chile, 39°S

Sébastien Bertrand [a, 1, *], François Charlet [b], Emmanuel Chapron [b, c], Nathalie Fagel [a] and Marc De Batist [b]

[a] Clays and Paleoclimate Research Unit, Department of Geology, University of Liège, Allée du 6 août, B18, 4000 Liège, Belgium

[b] Renard Centre of Marine Geology (RCMG), University of Ghent, 9000 Ghent, Belgium

[c] Geological Institute, ETH Zentrum, Zürich, Switzerland

[1] Present address: Marine Chemistry and Geochemistry, Woods Hole Oceanographic Institution, MS#25, MA 02543, Woods Hole, USA

* Corresponding author, e-mail: sbertrand@whoi.edu, tel: +1-508.289.3410, fax: +1-508.457.2193

Abstract

South-central Chile is one of the most geodynamically active areas in the world, characterised by frequent volcanic eruptions and numerous earthquakes, which are both recorded in lake sediments. In Lago Icalma (39°S), long piston and short gravity coring, as well as 3.5 kHz high-resolution seismic profiling, has been carried out in order to study the Holocene sedimentary infill of the lake, with a special focus on earthquake-triggered deposits. Macroscopic description of sediment cores and detailed grain-size analyses allow us to identify four types of seismically-induced deposits, or “seismites”: slump deposits, chaotic deposits, turbidites s.s. and homogenites. Homogenites are characterized by the occurrence of three distinct units on grain-size profiles (coarse base, thick homogenous unit topped by a thin layer of very fine sediment) and by the typical distribution of the grain-size parameters in a skewness-sorting diagram, while turbidites s.s. are characterized by a continuous fining upward trend.

Radiocarbon, ^{210}Pb dating, and tephrochronology allow us to demonstrate that the regional seismotectonic activity was probably very high between 2200 and 3000 cal. yr. BP as well as between 7000 and 8000 cal. yr. BP and that none of the historically documented earthquakes have triggered any seismite in Lago Icalma. The most recent seismite recognized in the sediments of Lago Icalma is a slump deposit dated at 1100 ± 100 AD, i.e. older than the period covered by historical records. The remarkable record of seismites between 2200 and 3000 cal. yr. BP is probably influenced by a major eruption of Sollipulli volcano at 3000 cal. yr. BP, which has rejuvenated the stock of terrigenous particles available for erosion, by depositing a thick layer of pumices all over the watershed of Lago Icalma and by clearing the vegetation covering the volcanic ash soils. This paper demonstrates that the record of seismically-triggered deposits in lake sediments is not only controlled by the intensity of the triggering earthquake and the occurrence of unstable sediment along the lake slopes but also by the presence of particles available for erosion/remobilisation in the watershed.

Keywords: Seismite, turbidite, homogenite, geodynamic activity, lake sediments

1. Introduction

Due to its location near the subduction zone of the Nazca plate under the South American plate, south-central Chile is characterized by a strong geodynamic activity. This characteristic is responsible for intense earthquakes and major volcanic eruptions. Since 1520 AD, 22 earthquakes with an estimated magnitude > 7 have been recorded in the Lake District region between 37 and 42°S (Lomnitz, 1970, 2004; Lorca and Recabarren, 1997), causing destruction of buildings, triggering volcanic eruptions and generating landslides in the Andes, tsunamis in the Pacific Ocean and seiches in regional lakes (Rothé, 1961; Silgado, 1985; Beck et al., 1998) (Fig. 1). The strongest earthquake ever recorded occurred in Chile on 22 May

1960 off Valdivia (Cisternas et al., 2005). This 9.5 magnitude earthquake killed more than 2000 people, left 2 million homeless, caused heavy damage in several coastal cities and triggered a tsunami in the Pacific Ocean that caused destruction as far as Hawaii and Japan (Cisternas, 2005 and references therein). Inland, this earthquake triggered numerous landslides in the Southern Cordillera de Los Andes, as well as a seiche with a 60 cm high wave in Lago Puyehue (40°S). It was also responsible for the eruption of the Puyehue-Cordon de Caulle volcano (Tazieff, 1960, 1962; Rothé, 1961; Veyl, 1961; Lara et al., 2004).

It is now well known that such earthquakes with a magnitude ≥ 6 can trigger *in situ* deformation and/or destabilization of lake sediments (Inouchi et al., 1996; Lignier, 2001), especially in basins dominated by high inputs of terrigenous and volcanoclastic material (Einsele et al., 1996). In consequence, lake sediments have frequently and successfully been used as archives of past seismic activity (Doig, 1986, 1990, 1991; Inouchi et al., 1996; Siegenthaler et al., 1987; Hibsch et al., 1997; Chapron et al., 1999; Shiki et al., 2000; Schnellmann et al., 2002). Moreover, Cisternas et al. (2005) have recently demonstrated that accurate reconstructions of the recurrence time and magnitude of the earthquakes preceding the giant 1960 earthquake of Chile are essential to infer the magnitude of future seismic events in the area.

In this paper, we analyze high resolution grain-size data obtained on sediment cores and 3.5 kHz seismic profiles from Lago Icalma (Southern Chile, 39°S) in order to reconstruct the Holocene seismotectonic activity of the Southern Andes. Combined with mineralogical data, these results allow us to infer the origin of the remobilized sediment and to reconstruct the depositional pattern of the seismites.

2. Location

Lago Icalma is a small (11.65 km^2) but deep (135 m) oligotrophic lake from the IX region of Chile (Parra *et al*., 1993), located in the Cordillera de Los Andes at an elevation of 1140 m (Fig. 1). This lake is believed to occupy a glacial over-deepened valley and its main basin is delimited by glacial rock-bars to the West and by moraines to the East (Mardones *et al*., 1993). The lake catchment covers 147 km^2 and is surrounded by several active volcanoes (i.e., Llaima, Lonquimay and Sollipulli), with Llaima volcano being one of the most active volcano of South America (González-Ferrán, 1994). The lake catchment has been shaped by north-south tectonic faults, volcanism and glaciations (Mardones *et al*., 1993; Suárez and Emparan, 1997). The bedrock is characterized by Jurassic granodiorites, basalts and sedimentary rocks, covered by soft Holocene volcanic ashes, several meters thick and intercalating two pumice layers emitted by Llaima volcano (Llaima pumice) in 10,000 cal. yr. BP and by Sollipulli volcano (Alpehue pumice) in 3000 cal. yr. BP (Naranjo and Moreno, 1991; Naranjo et al., 1993; Suárez and Emparan, 1997; De Vleeschouwer et al., 2005). The catchment area above the N-W flank of the lake is an unstable area (Mardones et al., 1993) characterized by steep and deeply scoured canyons (Fig. 2).

Lago Icalma is fed by Rio Icalma in the South, forming the main delta, and by Rio Huillinco in the West, flowing into the Laguna Chica de Icalma (Fig. 2). The outlet of Lago Icalma (Rio Rucanuco) cross-cuts a small dump moraine and forms, together with the outlet of Lago Galletue, the source of Biobio river (Fig. 1). Annual regional precipitation varies between 1180 and 3000 mm/yr and the area is characterized by high temperature changes, with extremes of -6°C during the winter and 29°C during the summer (Mardones *et al*., 1993; Parra *et al*., 1993).

Due to the geographical setting of Chile and to the concentration of the population in the central valley and in a few coastal cities, earthquakes that hit the Andes are poorly known.

Except for the last decades, the magnitude of past Chilean earthquakes is derived from damages that affected coastal cities but many more historical events are believed to have occurred in remote and unpopulated areas (Lomnitz, 2005).

3. Material

3.1. Coring and core processing

After a preliminary seismic investigation of the whole sedimentary infill of Lago Icalma (Charlet et al., 2003), two sites were selected for the collection of both long and short sediment cores. The first coring site (ICA-I) is located at 77.3 m depth, north of the main glacial rock-bar that divide the lake into two sub basins (Fig. 2). The ICA-II site is located in the central and deepest part of the lake, at a depth of 134.7 m (Fig. 2). In 2001-2002, a coring campaign, using a 3 m long piston coring system operated from an Uwitec platform, collected a series of 6 cm inner diameter cores at ICA-I and ICA-II sites. Moreover, a classical short gravity coring device was used to collect 5 short cores at each coring site. Core sections were then opened, photographed, described (colour, grain-size, structure and contacts) and scanned for magnetic susceptibility with a Bartington MS2E point sensor every 5 mm. Once all processed, the 3 m long sections were correlated using magnetic susceptibility results and distinct layers described macroscopically. The composite lithological columns (ICA-I: 776.9 cm, ICA-II: 816.15 cm) were then used for sampling: the working half of each composite core was subsampled in 1 cm thick slices for a multi-proxy study while the archive halves have been used for grain-size analyses.

3.2 Lithology

The sediment of ICA-I and ICA-II cores is composed of olive grey to dark yellowish brown silts alternating with coarse and dark sandy material (Fig. 3). The silty sediment is rich in diatoms and has a homogeneous to slightly laminated texture. In ICA-I core, the total thickness of the coarse deposits reaches 345 cm, i.e. 45% of the total length of the core, while the dark coarse particles constitute 23% of ICA-II core. Both cores also contain macroscopic wood remains and pumices (Fig. 3).

Microscopically, the coarse fraction (> 250 μm) of the sediment contains volcanic scoriae, opaque minerals, volcanic glasses and organic remains. Particles with a size between 250 and 50 μm are dominated by volcanic scoriae, volcanic glasses and various volcanic minerals (plagioclase, pyroxene, olivine …). The finest (< 50 μm) fraction of the sediment contains volcanic glasses, allophane, diatoms and minerals superficially altered into allophane.

3.3 Radiocarbon, ^{210}Pb dating and tephrochronology

In order to date the main event deposits in each of the cores, ten samples (bulk samples and wood remains, Tab. 1 and Fig. 3) were AMS radiocarbon dated at the Poznan Radiocarbon Laboratory (Czernik and Goslar, 2001). Moreover, an *in situ* pumice layer recognized in both cores (ICA-I, 398-409 cm and ICA-II, 513-531 cm) has been used as a tephrochronologic marker. After a detailed mineralogical and geochemical study, these pumices have been attributed to the Alpehue eruption of Sollipulli volcano at 3000 cal. yr. BP (Naranjo et al., 1993; De Vleeschouwer et al., 2005). The volcanic ash soils around Lago Icalma contain a second pumice layer, attributed to an eruption of Llaima volcano at 10,000 cal. yr. BP (Naranjo and Moreno, 1991; De Vleeschouwer et al., 2005). This pumice layer, with its typical mineralogy and geochemistry, has not been found in our sediment cores, arguing that the base of the cores is younger than 10,000 cal. yr. BP.

To accurately date the recentmost deposits, ^{210}Pb and ^{137}Cs concentrations were analysed in short cores ICA-I-P2 and ICA-II-P1 (Arnaud et al., in press). Because ^{210}Pb profiles are disturbed by event deposits, data corresponding to disturbed layers were removed from ^{210}Pb profiles and a simple ^{210}Pb decay model (CFCS) has been used to infer the mean accumulation rate of the continuous sedimentation (Arnaud et al., in press). This method, providing an accurate age-depth model for the last 150 yrs, has been extended to the base of the pilot cores, with the aim to estimate the age of the numerous historical instantaneous deposits (e.g., Arnaud et al., 2002; Nomade et al., 2005) (Fig. 3)

4. Methods

4.1 Grain-size

Grain-size measurements were performed every 2 cm on bulk sediment using a laser diffraction particle analyser Malvern Mastersizer 2000 which has a detection range of 0.02-2000 µm. Samples were introduced into a 100 ml deionised water tank free of additive dispersant, split with a 2000 rpm stirrer and disaggregated by sonication (Hydro S dispersion cell). Sample quantity was adjusted in order to obtain a laser beam obscuration between 10 and 20 %. Grain-size parameters are averaged over 10,000 scans. Samples containing grains coarser than 420 µm have been analysed by a combination of laser diffraction and sieving methods. Distribution parameters have been calculated following Folk and Ward (1957):

- Mean: $M_z = \dfrac{\phi_{16} + \phi_{50} + \phi_{84}}{3}$

- Sorting: $\sigma_I = \dfrac{\phi_{84} - \phi_{16}}{4} + \dfrac{\phi_{95} - \phi_5}{6{,}6}$

- Skewness: $Sk_I = \dfrac{\phi_{16} + \phi_{84} - 2(\phi_{50})}{2(\phi_{84} - \phi_{16})} + \dfrac{\phi_5 + \phi_{95} - 2(\phi_{50})}{2(\phi_{95} - \phi_5)}$

- Kurtosis: $K_G = \dfrac{\phi_{95} - \phi_5}{2.44(\phi_{75} - \phi_{25})}$

4.2 Mineralogy

Bulk and clay mineralogy were analysed by X-ray diffraction (XRD) on a Bruker D8-Advance diffractometer with CuKα radiations. Bulk samples taken every 10 cm were powdered to 100 µm using an agate mortar. An aliquot was separated and mounted as unoriented powder by the back-side method (Brindley and Brown, 1980). The powder was submitted to XRD between 2° and 45° 2θ. The data were analysed in a semi-quantitative way following Cook *et al.* (1975). The intensity of the principal peak of each mineral was measured and corrected by a multiplication factor. For amorphous material, a mean correction factor was obtained from diffraction results on mixtures of known quantities of amorphous material and quartz. We calculated a mean correction factor of 75, applied to the maximum of the broad diffraction band at 3.7 Å. For clay mineralogy, oriented mounts were realized by the "glass-slide method" (Moore and Reynolds, 1989) and subsequently scanned on the diffractometer. Slides containing crystallised clays after air drying were scanned two times more, once after ethylene-glycol solvation during 24 h and once after heating at 500°C for 4 h. As amorphous clays are abundant in the samples, only the presence or absence of crystalline clays is indicated.

4.3 Seismic reflection data acquisition

In Lago Icalma, about 75 km of very high resolution reflection seismic profiles (Fig. 2) were recorded using a GeoAcoustics 3.5 kHz subbottom profiler, essentially in the main basin, but also on the central platform (PU-I coring site) and in the adjacent western basin (Charlet et al., 2004). Moreover, two dense grids were acquired at the two main coring sites. The 3.5 kHz seismic profiler was composed of a 132B transducer array, a 5430A transmitter and a 5210A receiver, and it was mounted on a specifically designed cataraft that was towed behind the Huala-2 research vessel (Universidad Austral de Chile, Valdivia). Data were recorded digitally using an Elics Delph-2 seismic acquisition system, and seismic interpretation was done on an SMT Kingdom Suite system. The 3.5 kHz source penetrated the upper 15 m of sediment with a resolution of about 20 cm. Several seismic facies have been identified according to the seismic parameters (amplitude, frequency) and to the continuity and geometry of the reflections.

5. Results

5.1 Grain-size

Grain-size distributions of the sediment from ICA-I and ICA-II cores are characterized by a very low proportion of clay (< 2 µm) (Figs 4 and 5). The percentages of silt (2-63 µm) and sand (> 63 µm) reflect the different lithologies that can be grouped into two populations: (1) fine lake sediment (mean 20-25 µm), dominated by silt (80-95 %) and containing 5 to 20 % of sand; and (2) coarse sediment (mean 100-500 µm) characterized by a low proportion of silt (< 30 %) and by a high proportion of sand.

5.2 Magnetic susceptibility

Magnetic susceptibility values are generally high for the sediments of ICA-I core (391 ± 266.10^{-6} S.I.). Extreme values are 28 and 1378.10^{-6} S.I., with the maxima being related to sand layers, especially between 150 and 400 cm (Fig. 4). In ICA-II core, magnetic susceptibility values are in general lower than in ICA-I core (254 ± 142.10^{-6} S.I.). Lower and upper limits are 16 and 959 10^{-6} S.I., respectively. As in ICA-I core, the highest values are related to sand layers (Fig. 5).

5.3 Mineralogy

The bulk mineralogy of ICA-I core (Fig 4) is dominated by amorphous particles (52 ± 13 %) and plagioclase (29 ± 9 %). Secondary minerals are pyroxene (8 ± 3 %), quartz (4 ± 4 %), olivine (3 ± 2 %) and amphibole (3 ± 3%). The bulk mineralogy of ICA-II core is relatively similar (Fig. 5): amorphous particles (64 ± 9 %), plagioclase (24 ± 7 %), pyroxene (8 ± 3 %) and traces of quartz (2 ± 1 %) and olivine (2 ± 2 %). Amphibole has only been detected in one sample (465 cm). In both cores, the amorphous particles comprise amorphous clays (allophanes), volcanic glasses, amorphous silica and organic matter.

Clay diffractograms have revealed the omnipresence of non-crystallised clay particles (allophanes). Crystallised clay minerals, containing kaolinite, illite and vermiculite, only occur in very low proportion (max. 25 cps on diffractograms). In ICA-I core, the samples containing crystallised particles are located between 200 and 400 cm, in relation with the decrease of total amorphous particles in bulk mineralogy. In ICA-II core, only two samples contain crystallised clay minerals (455 and 465 cm).

6. Recognition and characterization of event deposits

6.1 Event deposits recognized in the sediment cores of Lago Icalma

Except for *in situ* tephras, which are characterized by their sharp contact with the host sediment and by their generally homogenous grain-size throughout the deposit, four types of event deposits can be identified. These deposits, intercalated in silty host sediments, have been identified on the basis of their typical structural and textural characteristics:

- Slump deposit (S): sediment layer of distinct lithology, with oblique and/or curved bedding configuration, included in a silty matrix. This deposit is not characterized by a typical grain-size distribution nor by a typical magnetic susceptibility signature. The main criterion for recognition is the structure of the slumped layer (Typical examples: ICA-I-P2, 39 – 43 cm and ICA-II-P1, 38 – 43 cm, Fig. 3).
- Turbidite s.s. (T): fining upward deposit composed of 2 units: (1) a dark and fining upward sandy base, grading into an overlying (2) silty fining upward unit. The coarse

sandy base, sometimes bounded to the underlying host sediment by an erosive contact, shows high magnetic susceptibility values. The typical recognition criterion is the fining upward of the entire sequence. (Typical example: ICA-I, 469-480 cm).

- Homogenite (H): sedimentary sequence composed of 3 units: (1) a coarse, dark and fining upward base, sometimes containing mud pebbles, pumices or wood fragments. This unit overlies the host sediment across an erosive contact and is gradually overlain by (2) a homogenous silty layer. This unit, remarkably free of sedimentary structures, sometimes contains macro-debris of organic matter. The thickness of this unit generally reaches half of the whole sequence. The sequence is capped by (3) a thin layer of very fine sediment, generally characterized by a light colour. The magnetic susceptibility profiles are generally conform to the mean grain-size curves. This definition of the homogenite is in agreement with the original description by Kastens and Cita (1981) and with that of Sturm et al. (1995). The main recognition criterion is the occurrence of the three units, easily differentiated by grain-size analyses. (Typical examples: ICA-I 100-155 cm, ICA-I 640-675 cm and ICA-II 108-313 cm).
- Chaotic deposits (C): this term is used for describing highly disturbed deposits consisting of a mixture of sandy layers included in a finer matrix. They have no typical sedimentary structure. The grain-size and magnetic susceptibility values are highly variable and depend on the proportions of coarse particles (Typical example: ICA-I, 314.3 - 326.8 cm).

6.2 Details of the textural properties of homogenites and turbidites

The homogenites are the best developed event deposits recorded in the sediment cores of Lago Icalma. In order to discuss their depositional pattern, their textural characteristics are detailed in figures 6, 7 and 8 and compared to those of turbidites (fig. 9).

6.2.1 Homogenites

The H_1 and H_2 homogenites, both recorded in ICA-I core (Fig. 6), show the three units typical for homogenites: (1) a coarse fining upward black sandy base in erosive contact with the underlying host sediment, (2) a thick homogenous silty unit with a very constant grain-size and (3) a thin layer of fine clayey silts. These three units clearly stand out in macroscopic descriptions and in the mean-grain size profiles. In these two examples, the magnetic susceptibility curve is roughly similar to the sand content and can be used as a first rapid criterion to recognize homogenites (Fig. 6). The only exception occurs at the very bottom of the homogenites, where low magnetic susceptibility values are reflecting the high porosity of the coarse-grained deposits. Textural parameters show that the coarse sand at the base of the sequences has been deposited rapidly under high velocity and turbulent currents (high values of mean and kurtosis and positive skewness). The high variability of the sorting at the base of H_1 homogenite could reflect different pulses of the gravity current. In the homogenous unit, the skewness values stabilize near 0, indicating a stabilisation of the energy of the depositional environment. The fine particles deposited in the last unit are characterized by a very low mean grain-size and a negative skewness, arguing for a slow settling. In a skewness-sorting diagram, the values corresponding to the three units are typically grouped into three distinct populations, what seems to be a typical characteristic for homogenites. The evolution of these values in the skewness-sorting diagram argues for an energy of the depositional environment that is decreasing by steps, with a long stabilization phase during the deposition of the homogenous unit.

The H_0 homogenite (ICA-II) is the thickest event deposit (205 cm) described in the Icalma sediment cores (Figs. 7 and 8). Its important thickness allows a very detailed study of its textural parameters. The coarse sandy base of the H_0 homogenite contains debris of pumices and wood fragments, the size of which reaches 3 cm. This unit is overlain by a 1 m thick silty homogenous unit containing some organic debris. The sequence is topped by a 5 cm thick layer of clayey silt. These three units are clearly differentiated by grain-size and magnetic susceptibility, except for the basal unit showing low MS values for the samples containing highly vesiculated pumices and wood fragments. As for the H_1 and H_2 homogenites, the textural parameters agree for a sequence deposited in an environment of step-wise decreasing energy. The only exception to this observation is the sorting and skewness values related to the pumice-rich sediments at the base of the sequence. In a skewness-sorting diagram (Fig. 8), the representative points are clearly grouped, one of the most striking features being the dense grouping of data representing the homogenous unit. The only exception to the overall trend from high values of skewness and sorting to negative values of skewness and low values of sorting is the very high sorting values of the pumice-rich sediments. This is due to the settling properties of pumices, which need to be water-saturated before sinking. Because small pumices are faster saturated with water than coarser ones, pumice deposits generally shows a coarsening upward texture (White et al., 2001).

6.2.2 Turbidites

In the previous paragraph, we demonstrated that the typical criteria to distinguish homogenites are: (1) 3 characteristic units that clearly stand out in macroscopic descriptions and grain-size profiles, and (2) the identification of these 3 units when representative points are plotted in a skewness-sorting diagram, with an impressively dense grouping of the points representing the homogenous unit. To compare these results with event deposits identified as turbidites, the figure 9 shows the textural parameters of T_1 and T_2 turbidites, described in ICA-I (469-480 cm) and ICA-II (718-734 cm) cores, respectively.

Macroscopic description and mean grain-size show a gradual evolution from a coarse sandy base to fine silts, especially for T_1 (Fig. 9). The transition between the two units is sharper in T_2 than in T_1 and a thin fine silt layer occurs at the top of the T_2 sequence, making it intermediate between a typical turbidite s.s. and a homogenite. Sorting and skewness are decreasing upward, except for T_2 for which sorting increases in the second unit. The most striking difference between T_1 turbidite and the homogenites described in the previous paragraph is the continuity of the representative points in a skewness-sorting diagram, arguing for a sequence deposited in an environment with a gradually decreasing energy (velocity and turbulence). In the skewness-sorting diagram, the T_2 turbidite also seems intermediate between a turbidite s.s. and a homogenite.

6.3 Geometries of the event deposits

In order to investigate the spatial distribution of the thickest event deposits, the remarkable seismic reflections observed on seismic profiles passing through ICA-I and ICA-II coring sites (Figs 10 and 11) have been compared with the lithology of the sediment cores. The cores were tied to the seismic profiles assuming an acoustic velocity of 1450 m/s. The resolution of the seismic cross-sections obtained with the pinger source (3.5 kHz) being ~ 20 cm (Charlet et al., 2004), only the sedimentary events thicker than ~ 50 cm can be accurately detected and mapped. In general, a structurally homogenous deposit appears on a seismic profile as a unit with a transparent seismic facies, or as low-amplitude reflections (Siegenthaler et al., 1987, Chapron et al., 1999, van Rensbergen et al., 1999; Schnelmann et al., 2002).

On the seismic profile ical73 passing through ICA-I coring site, several lithological units are discerned (Fig. 10). The two homogenites H_1 and H_2 are represented by low amplitude reflections, and extend over most of the deepest part of the sub basin. An intermediate low amplitude reflection with a slightly chaotic pattern covering continuous high amplitude reflections in the deepest part of the sub basin seems to correlate with a succession of chaotic deposits in ICA-I between 250 and 350 cm (Figs. 4 and 10). These reflections are laterally evolving into lens-shaped bodies containing contorted to chaotic reflections that are interpreted as a mass flow deposit (MFD5). In the middle of the core, the *in situ* pumice layer, related to the Alpehue eruption of Sollipulli caldera in 3000 cal. yr. BP is associated with poorly continuous low amplitude reflections that are slightly contorted.

On the seismic cross-section ical88 passing through ICA-II coring site (Fig. 11), the low amplitude facies due to the homogenous unit of H_0 turbidite (H_{0h} in figure 7) is clearly distinguished and followed laterally in the deep basin. This thick facies in the deepest part of the basin is quickly pinched-out laterally in all directions. The coarse sandy base of the homogenite corresponds to several locally wavy high amplitude reflections in the centre of the basin but becomes more chaotic towards the central basin edges. Finally, the two other low-amplitude reflections observed on the ical88 profile are caused by the *in situ* Alpehue pumice deposit and by the numerous turbidites and chaotic deposits occurring at the base of ICA-II core (Figs 5 and 11).

The dense grid of seismic profiles in Lago Icalma (approximately 75 km of profiles in the main basin of the lake (9.8 km²) – Charlet et al., 2004) allows to laterally follow the reflections corresponding to the two thickest units of the H_0 homogenite (H_{0b} and H_{0h}) and to map their spatial distribution. The 3D mapping using the seismic data demonstrates that the H_0 homogenite (in ICA-II) is the lateral continuity of the H_1 homogenite (in ICA-I), however better developed because of its location in the central and deepest part of the lake. The relatively small thickness of the H_1 homogenite (55 cm) does not allow to differentiate the coarse basal and the homogenous units on the seismic data. Where the thickness of both units was sufficient to be accurately distinguished on seismic profiles, these two units were picked and their thickness was mapped. This mapping indicates that the sediments constituting the H_1 homogenite originate from the northern slopes of the basin, probably in continuity of the canyons draining this part of the catchment (Figs. 12 and 2). The coarse basal unit of the H_0 homogenite (H_{0b}) develops several depocenters at the foothill of the steep sublacustrine slopes and occurs nearly everywhere below 120 m depth, with a minimum thickness in the central and deepest part of the lake (Fig. 12). Its thickness reaches more than 6 ms TWT (4.8 m) at the foothill of the steep sublacustrine slopes. The isopach map in Fig. 12 also shows that the homogeneous H_{0h} unit is confined to the deepest part of the lake, where its maximum thickness reaches more than 2.5 ms TWT (2 m). The total volume of the homogenous unit has been calculated as 463.000 m^3.

These characteristics of the spatial distribution of the H_0 homogenite are very similar to the observations made in the Mediterranean Sea by Cita and Rimoldi (1997) during the seismic mapping of the 3500 yr. BP tsunami-induced homogenite. The coarse basal unit being the thickest nearby the steep slopes of the lake bottom could indicate both sub aerial and sub aquatic sediment sources for this major event (Fig. 12). The most complete sequence of the H_0 homogenite is recorded in the central and deepest part of the lake where the coarse basal unit and the homogenous unit have approximately the same thicknesses.

7. Chronology of the event deposits

For the upper part of the sedimentary section, the extrapolation of the ^{210}Pb CFCS age-depth model gives an age for the first event deposit (slump deposit) occurring at ~ 40 cm in ICA-I and ICA-II cores of 1200 ± 200 AD and 1400 ± 100 AD, respectively (Fig. 3). For the same slump deposit, the interpolation of the first radiocarbon date with the age of the top of the core (2001 AD) gives an age of 1060 ± 60 BP (ICA-I) and 1000 ± 50 BP (ICA-II). Even if the dates obtained for both events, and by both dating methods, are not in perfect agreement, several observations evidence that this event deposit is synchronous in both cores: (1) the visual lithostratigraphic correlations (Fig. 3); (2) the tephrostratigraphic correlations between ICA-I and ICA-II short cores (De Vleeschouwer, 2002); (3) the similar depth of this event in both cores, as well as in other short cores collected all over Lago Icalma (Bertrand, 2005); (4) its large spatial distribution (Bertrand, 2005); and (5) its uniqueness in Lago Icalma sediments. We can thus assume that this unique key horizon has been deposited in 1100 ± 100 AD, which is older than the period covered by historical records. This age is strikingly consistent with the date obtained by Cisternas et al. (2005) on a tsunami sand layer recorded in Rio Maullin Estuary (Chile, 42°S).

The age of the older sedimentary events recorded in the ICA-I and ICA-II long cores was carefully estimated using the radiocarbon dates and the tephrochronological marker at 3000 cal. yr. BP (Alpehue pumice). A continuous age-depth model based on these dates can not be applied because of the large number of instantaneous deposits (both gravity reworked and fallout tephra deposits) affecting the sedimentation rates.

When comparing the stratigraphic relationships between the Alpehue pumice layer and the nearest radiocarbon dates (Fig. 3), an incompatibility between both dating methods is highlighted. The *in situ* pumice layer is stratigraphically encompassed by two samples dated at 4760 ± 110 cal. yr. BP (40 cm under the pumice layer in ICA-I core) and 3690 ± 140 cal. yr. BP (above the pumice layer in ICA-II core). Radiocarbon ages are several hundreds years older than the well-constrained true age of the pumice layer (3000 cal. yr. BP, Naranjo et al., 1993; De Vleeschouwer et al., 2005). It seems that this difference is due to an ageing of the radiocarbon dates obtained on lake sediments, probably due to the incorporation of juvenile carbon emitted by the highly active regional volcanoes (Hajdas, 1993; Calderoni and Turi, 1998). When there is an incompatibility between the age of the pumice layer and the radiocarbon dates, the age of the pumice layer is preferentially used (Fig. 3).

Also, we have discarded the radiocarbon dates obtained on bulk sediment and on the organic macro-debris in the H_0 and H_1 homogenites because of their reworked origin (ICA-I 131.5 cm, ICA-II 140 cm and ICA-II 236.5 cm). Finally, we have used the absence of the Llaima pumice layer in both cores (Naranjo and Moreno, 1991; De Vleeschouwer et al., 2005) as an indicator that the base of the cores is younger than 10,000 cal. yr. BP.

Considering these remarks, an age has been attributed to each sedimentary event described in Lago Icalma sediment cores, taking into account the mean sedimentation rates of the sediments deposited continuously between the dated samples (Fig. 3). The thickness of these deposits has been plotted against their calculated age, allowing us to compare the event stratigraphy of both cores (Fig. 13).

Figure 13 clearly demonstrates that both cores have recorded a large number of sedimentary events between 3000 and 2200 cal. yr. BP, with the thickest event deposit of each core (H_1 and H_0 homogenites) dated at 2200 cal. yr. BP. The latter observation supports the idea that emerged from the interpretation of the seismic profiles, stating that the H_0 and H_1 homogenites are contemporaneous. Figure 13 also shows that ICA-I site has recorded several relatively thin turbidites at 4000 and 5000 cal. yr. BP, that do not have any equivalent in ICA-II core. In addition, between 8000 and 7000 cal. yr. BP, one turbidite and two chaotic deposits have been recorded in ICA-II core. Given the error on the age-depth model at the base of the cores, one of them can be contemporaneous with the H_2 homogenite recorded in ICA-I core.

8. Discussion

8.1 Sediment origin

Because of the small size of allophane and diatoms, the mineralogy of the sediment largely depends on its grain-size, the finest fraction being enriched in amorphous particles (Fig. 4 and 5). The bulk mineralogy of both cores, dominated by amorphous particles and plagioclases, is typical for the regional Holocene volcanic ash soils (Laugenie, 1982; Bertrand, 2005), evidencing that these soils constitute the main source of sediments to the lake.

8.1.1. Difference between ICA-I and ICA-II

While the mineralogy of the ICA-II core is composed for 98 % of amorphous particles, plagioclase and pyroxene, the mineralogy of ICA-I core is more diversified, with significant amounts of quartz, olivine, amphibole and crystallised clay minerals, especially in the coarse layers (Figs 4 and 5). However, quartz, amphibole and crystallised clay minerals are not typical for the regional volcanism and do not occur in the regional volcanic ash soils. The only places where amphibole, quartz and crystallised clay minerals occur in the watershed of Lago Icalma are (1) the pre-Holocene coarse and relatively soft moraine deposits, which are covered by several meters of volcanic ashes and (2) some rocks constituting the substratum of the watershed (Bertrand, 2002). In consequence, while sediments from the ICA-II coring site only originate from the thick cover of regional volcanic ash soils, the source of sediment for ICA-I coring site is a mixture of moraine sediments and volcanic ash soils. This difference between the two coring sites is due to the proximity of ICA-I to the sediment sources in the watershed (see Fig. 2), making the sediments of ICA-I core coarser than in ICA-II. This coarser grain-size of ICA-I sediments implies a higher contribution of the coarse moraine sediment, that, compared to the light volcanic ash sediments, are too heavy to reach ICA-II site.

8.1.2 Sources of H_0–H_1 homogenite sediments

Smear slides from the homogeneous unit of the H_0 homogenite have demonstrated the presence of diatoms, evidencing that the major part of these fine sediments originate from the reworking of previously deposited lake sediments. Their main source is probably located in the north-western part of the lake, where the lake bottom is characterized by slopes reaching 20°. This interpretation is in agreement with the isopach map of the H_{0b} unit (Fig. 12).

Radiocarbon ages obtained on organic-rich samples from the H_0 and H_1 homogenites agree with this hypothesis. Indeed, the H_0-H_1 homogenite, dated at 2200 cal. yr. BP, contains two types of organic matter: (1) wood remains dated at 2270 ± 90 and 2535 ± 185 cal. yr. BP, i.e. wood that died before the deposition of the homogenite and that was included in soil sediments, and (2) organic-rich sediment, dated at 4190 ± 110 cal. yr. BP, i.e. reworked from previously deposited lake sediment. These data confirm that the sediment constituting the H_0-H_1 homogenite is a mixture of particles coming from the watershed and from previously deposited lake sediment, and this is probably the case for most of the sedimentary events recorded in Lago Icalma.

8.2 Triggering mechanisms and timing of the regional seismotectonic activity

Because gravity reworking in lakes could be initiated by different processes, one of the strongest argument to assign a seismic triggering to a sedimentary event characterized by specific grain-size and geometrical signatures is to correlate it with a well-documented historical earthquake (Siegenthaler et al., 1987; Doig, 1990; Shiki, 1996; Inouchi et al., 1996; Chapron et al., 1999; Schnellmann et al., 2002; Arnaud et al., 2002; St-Onge et al., 2004; Nomade et al., 2005). In that case, paleo-earthquakes can then be proposed as a triggering mechanism for similar gravity reworked deposits (i.e. seismites) occurring further back in time, when no more historical data is available. The second strong argument to assess a seismic triggering to a slope failure and the development of gravity reworking is the concomitant occurrence of related deposits in several basins or sub basins (Doig, 1991; Schnellmann et al., 2002).

In this study, some of the thick sedimentary events of Lago Icalma are bearing striking similarities with previously documented earthquake-triggered homogenites and turbidites in marine and lacustrine environments (Kastens and Cita, 1981; Siegenthaler et al., 1987; Inouchi et al., 1996; Chapron et al., 1999; Cita and Aloisi, 2000). These sedimentary events in Lago Icalma are older than available historical chronicles (Lorca and Recabarren, 1997; Lomnitz, 2005) and therefore they can not be directly correlated to any former earthquakes documented in the Chilean Lake District. However, given (i) the strong geodynamic setting of the study area, (ii) the synchronous development of these sedimentary events in both sub basins of Lago Icalma and (iii) the similarities of some of these sedimentary events with well-documented seismites in the literature, we interpret synchronous sedimentary events retrieved at coring sites ICA-I and ICA-II as seismites. While all the homogenites, slump and chaotic deposits retrieved at our coring sites can be interpreted as seismites, only the thick turbidites have an obvious seismic origin (Fig. 13). Thinner turbidites at site ICA-I (at 5000 and 6000 cal. yr. BP) may therefore result from other processes restricted to certain locations of the lake such as heavy rainfalls reactivating the steep canyons at the NW slopes of the lake catchment.

If these thick and synchronous deposits are true seismites directly linked to the regional seismic activity, their occurrence in Lago Icalma indicate that this part of the Southern Andes has been affected by a strong event in 1100 ± 100 AD, an intense seismotectonic activity between 3000 and 2200 cal. yr. BP, and a slightly less important one between 8000 and 7000 cal. yr. BP. These data therefore demonstrate that none of the numerous and intense historical earthquakes that affected the Chilean Lake District (see Fig. 1) has triggered a seismite in Lago Icalma. This can be explained either by (1) the unavailability of sediment available for remobilisation or by (2) the nature of regional earthquakes that affected Chile during the last 500 years.

However, the good record of the seismites between 3000 and 2200 cal. yr. BP could also be influenced by the Alpehue eruption of the Sollipulli volcano at 3000 cal. yr. BP, which rejuvenated the erodible stock of detrital particles, and hence, provided a lot of fresh material available for generating seismites. In addition, pumice fallouts due to this eruption, which are characterized by a thickness of 30 cm to 1 m in the watershed of Lago Icalma (Naranjo et al., 1993; De Vleeschouwer, 2002), have probably affected the regional vegetation, clearing the soil of most of its vegetal cover. Finally, the volcanic activity is probably not the only factor influencing the record of seismites in Lago Icalma. One must keep in mind that the suggested intense seismic activity that occurred between 3000 and 2200 cal. yr. BP has probably destabilized a large volume of soft sediment in the lake watershed, that has accumulated at the foot of the steep slopes, and was readily available for remobilisation in response of an intense earthquake in 2200 cal. yr. BP (H_0-H_1 homogenite). Since the sedimentary events are resulting from the destabilisation of soils and lake sediments, the size and the frequency of the seismites in Lago Icalma are not only related to the intensity of the seismo-tectonic activity, but they may also reflect the intensity of the volcanic eruptions in the study area.

8.3 Depositional history of the H_0 – H_1 homogenite: a conceptual model

For the deposition of the H_0 – H_1 homogenite, we propose that an intense earthquake has triggered the following processes (Fig. 14):

(1) The instable soft sediments accumulated at the foothills of the NW flank of the watershed (or higher up along the steep aerial slopes) and on the central peninsula are destabilized and move downslope as a massive landslide, right into the lake.

(2) The earthquake and/or the massive landslide provoke the destabilization of lake sediments previously deposited on steep slopes. These sediments generate a high density flow and the finest particles are resuspended, forming a suspension cloud.

(3) The earthquake, the impact of the landslide or the sublacustrine slope failure trigger a seiche (as it was observed in Lago Puyehue during the 1960 earthquake by Veyl (1961)). The seiche maintains the silty and clayey particles in suspension by oscillating the suspension cloud back and forth (Siegenthaler et al., 1987). The seiche is also capable of creating an underwater current able to transport sand size particles (Siegenthaler et al., 1987; Chapron et al., 1999). During this time, the high density flow slows down and most of the coarse particles settle down, with a fining upward and fining basinward texture. This deposit forms the coarse base of the homogenite, with pumices and wood fragments being included depending on their density.

(4) When the lake water oscillation wanes, the suspension cloud moves towards the centre part of the basin, where most of the the particles that were maintained in suspension settle down (Siegnethaler et al., 1987; Chapron et al., 1999). This produces a massive and homogenous deposit of silty particles characterized by a symmetrical grain-size distribution.

(5) Only the very fine particles (< 10 μm) remain in suspension in the water column

(6) The fine particles settle down, either after a relatively long time or during the turnover of the water column (Sturm and Matter, 1978), depending on the limnological conditions.

The mechanism that caused the seismo-turbidites in Lago Icalma is probably very similar, with as main difference that it did not create a seiche, leading to the absence of a typical homogenous unit. Moreover, due to the influence of lake geometry and water depth on the energy and amplitude of seiche waves (Sieghentaler, et al., 1987; Schnellmann et al., 2002), homogenites may laterally evolve to seismo-turbidites (e.g., H_2 homogenite at ICA-I site and T_2 turbidite at ICA-II site, which is texturally intermediate between homogenite and turbidite s.s.). Lateral differences can also be explained by variations in the velocity of the bottom current produced by the seiche waves, which is inversely proportional to the water depth (Sieghentaler, et al., 1987; Chapron et al., 1999).

9. Conclusions

Lago Icalma sediments contain a large number of seismites. Their occurrence is due to the highly active regional geodynamic setting, to the morphology of the lake basin, and to the high amount of frequently rejuvenated volcanoclastic particles, which are available for erosion/remobilisation in the watershed.

According to radiocarbon and ^{210}Pb dating, the youngest seismite recorded in Lago Icalma sediments is dated at ~ 1100 AD evidencing that no historical earthquake has triggered a seismite in the core sediments. Between 3000 and 2200 cal. yr. BP and during 8000-7000 cal. yr. the seismotectonic activity of the southern Andes was probably more intense, as evidenced by the numerous seismites recorded in Lago Icalma during these periods. However, the occurrence of several seismites in 2200-3000 cal yr. BP could also be influenced by a major eruption of Sollipulli volcano in 3000 cal. yr. BP that has increased the stock of erodible terrigenous particles by cleaning the soils from most of its vegetal cover and by depositing a 30 cm to 1 m thick pumice layer in the lake catchment.

Our results therefore show that the record of regional seismicity in Lago Icalma sediments and probably in lake systems in general, is not only controlled by the intensity of the seismotectonic activity and the stability of the subaqueous sediments, but also by the availability of erodible soft sediments in the watershed.

Acknowledgments

This research is supported by the Belgian OSTC project EV/12/10B "A continuous Holocene record of ENSO variability in southern Chile". We acknowledge Virginie Renson for laboratory assistance and Chrisitian Beck, Fabien Arnaud, Vincent Lignier, Xavier Boës and Alejandro Peña for their help during the coring mission. Thanks to Maria Mardones, Roberto Urrutia (U. of Concepción) and Mario Pino (U. of Valdivia) for their great logistic support during our fieldwork in Chile. The Bartington magnetic susceptibility meter has been cordially lent by Mike Sturm (EAWAG, Switzerland). We are grateful to André Rulmont and Etienne Juvigné, for providing kind access to the laser particle analyser and to the sieving material, respectively.

References

Arnaud, F., Lignier, V., Revel, M., Desmet, M., Beck, C., Pourchet, M., Charlet, F., Trentesaux, A., Tribovillard, N., 2002. Flood and earthquake disturbance of ^{210}Pb geochronology (Lake Anterne, NW Alps). Terra Nova 14 (4), 225-232.

Arnaud, F., Magand, O., Chapron, E., Bertrand, S., Boës, X., Charlet F., Mélières, M.-A., in press. Radionuclide dating (^{210}Pb, ^{137}Cs, ^{241}Am) of recent lake sediments in a highly active geodynamic setting (Lakes Puyehue and Icalma – Chilean Lake District). Science of the Total Environment.

Beck, S., Barrientos, S., Kausel, E., Reyes, M., 1998. Source characteristics of historic earthquakes along the central Chile subduction zone. Journal of South American Earth Sciences 11 (2), 115-129.

Bertrand, S., 2002. Caractérisation des apports sédimentaires lacustres de la région des lacs, Chili méridional (exemple des lacs Icalma et Puyehue). Unpublished Master thesis, University of Liège, Belgium.

Bertrand, S., 2005. Sédimentation lacustre postérieure au Dernier Maximum Glaciaire dans les lacs Icalma et Puyehue (Chili méridional) : Reconstitution de la variabilité climatique et des évènements sismo-tectoniques. Unpublished PhD thesis, University of Liège, Belgium.

Brindley, G. W., Brown, G., 1980. Crystal structures of clay minerals and their x-ray identification. Mineralogical Society Monograph, London, Vol. 5.

Bronk Ramsey C., 2001. Development of the Radiocarbon program OxCal. Radiocarbon 43 (2A): 355-363.

Calderoni, G., Turi, B., 1998. Major constraints on the use of radiocarbon dating for tephrochronology. Quaternary International 47-48, 153-159.

Chapron, E., Beck, C., Pourchet, M., Deconinck, J. F., 1999. 1822 earthquake-triggered homogenite in Lake Le Bourget (NW Alps). Terra Nova 11 (2/3), 86-92.

Charlet, F., Marchand, C., Volland, S., Pino, M., Urrutia, R., Mueller, J., Chapron, E., De Batist, M., 2003. Reflection-seismic study of six lakes in South-Central Chile (37°S-42°S): Lagos Laja, Lleulleu, Icalma, Villarrica, Puyehue & Todos Los Santos. Extended Abstract, *10° Congresso Geologico Chileno*, Concepcion, Chile, 10 p.

Charlet, F., Marchand, C., Bertrand, S., Chapron, E., Pino, M., Urrutia R., De Batist, M., 2004. Geophysical reconstruction of the sedimentary infill of Lago Icalma (39°S, Chilean Lake District) since the last deglaciation. GEOSUR extended abstracts, Bollettino di Geofísica teorica ed applicata 45 (supplement), 238-242.

Cisternas, M., Atwater, B.F., Torrejón, F., Sawai, Y., Machuca, G., Lagos, M., Eipert, A., Youlton, C., Salgado, C., Kamataki, T., Shishikura, M., Rajendran, C.P., Malik, J.V., Rizal, Y., Husni, M., 2005. Predecessors of the giant 1960 Chile earthquake. Nature 437, 404-407.

Cita, M.B., Aloisi, G., 2000. Deep-sea tsunami deposits triggered by the explosion of Santorini (3500 y BP), eastern Mediterranean. Sedimentary Geology 135, 181-203.

Cita, M.B., Rimoldi, B., 1997. Geological and geophysical evidence for a holocene tsunami deposit in the eastern mediterranean deep-sea record. Journal of Geodynamics 24 (1-4), 293-304.

Cook, H. E., Johnson, P. D., Matti, J. C., Zemmels, I., 1975. Methods of sample preparation and x-ray diffraction data analysis, x-ray mineralogy laboratory. In: Kaneps, A. G. (Ed.), Initial reports of the DSDP 28, Washington DC, 997-1007.

Czernik, T., Goslar, T., 2001. Preparation of graphite targets in the Gwilice radiocarbon laboratory for AMS ^{14}C dating. Radiocarbon 43 (2), 283-291.

De Vleeschouwer, F., 2002. Etude téphrostratigraphique de dépôts holocènes des bassins versants de deux lacs chiliens - exemple des lacs Icalma et Galletue (Chili, 38°S, 71°W). Unpublished master thesis, University of Liège, Belgium.

De Vleeschouwer, F., Juvigné, E., Renson, V., Naranjo, J. A., 2005. Mineral chemistry of Llaima pumice, Southern Chile: evidence of magma mixing. Geologica Belgica 8 (1-2), 135-144.

Doig, R., 1986. A method for determining the frequency of large-magnitude earthquakes using lake sediments. Canadian Journal of Earth Sciences 23, 930-937.

Doig, R., 1990. 2300 yr history of seismicity from silting events in Lake Tadousac, Charlevois, Quebec. Geology 18, 820-823.

Doig, R., 1991. Effects of strong seismic shaking in lake sediments, and earthquake recurrence interval, Témescaming, Quebec. Canadian Journal of Earth Sciences 28, 1349-1352.

Einsele, G., Chough, S. K., Shiki, T., 1996. Depositional events and their records - an introduction. Sedimentary Geology 104, 1-9.

Folk, R. L., Ward, W. C., 1957. Brazos river bar: a study in the signifiance of grain size parameters. Journal of Sedimentary Petrology 27 (1), 3-26.

González-Ferrán, O., 1994. Volcanes de Chile. Instituto Geografico militar, 635 p.

Hajdas, I., 1993. Extension of the radiocarbon calibration curve by AMS dating of laminated sediments of lake Soppensee and lake Holzmaar. Unpublished PhD thesis, ETH Zurich, Switzerland.

Inouchi, Y., Kinugasa, Y., Kumon, F., Nakano, S., Yasumatsu, S., Shiki, T., 1996. Turbidites as records of intense palaeoearthquakes in Lake Biwa, Japan. Sedimentary Geology 104, 117-125.

Hibsch, C., Alvarado, A., Yepes, H., Perez, V. H., Sébrier, M., 1997. Holocene liquefaction and soft-sediment deformation in Quito (Ecuador): a paleoseismic history recorded in lacustrine sediments. Journal of Geodynamics 24 (1-4), 259-280.

Kastens, K.A., Cita, M.B., 1981. Tsunami-induced sediment transport in the abyssal Mediterranean Sea. Geological Society of America Bulletin Part 1, 92, 845-857.

Lara, L.E., Naranjo, J.A., Moreno, H., 2004. Rhyodacitic fissure eruption in Southern Andes (Cordon Caulle; 40.5°S) after the 1960 (MW: 9.5) Chilean earthquake: a structural interpretation. Journal of Volcanology and Geothermal Research 138, 127-138.

Laugenie, C., 1982. La région des lacs, Chili méridional. Unpublished PhD thesis, Université de Bordeaux III, France.

Lomnitz, C., 1970. Major earthquakes and tsunamis in Chile during the period 1535 to 1955. Geologische Rundschau 59 (3), 938-960

Lomnitz, C. 2005. Major earthquakes of Chile: A historical survey, 1535-1960. Seismological Research Letters 75 (3), 368-378.

Lorca, E., Recabarren, M., 1997. Earthquakes and Tsunamis. Servicio Hidrográfico y Oceanográfico de la Armada de Chile - Departamento de Oceanografía, Programa de Geofísica Marina, Chile.

Lignier, V., 2001. Les sédiments lacustres et l'enregistrement de la paleosismicité - Etude comparative de différents cas dans la Quaternaire des Alpes Nord-Occidentales et du Tien-Shan Kyrghyze. Unpublished PhD thesis, Université de Savoie, France.

Mardones, M., Ugarte, E., Rondanelli, M., Rodriguez, A., Barrientos, C., 1993. Planificacion ecologica en el sector Icalma-Liucura (IX Region): proposicion de un metodo. EULA, Concepcion, Chile.

Moore, D. M., Reynolds, R. C. J., 1989. X-ray diffraction and the identification and analysis of clay minerals. Oxford University Press, Oxford.

Naranjo, J. A., Moreno, H., 1991. Actividad explosiva postglacial en el volcán Llaima, Andes del Sur (38°45'S). Revista Geológica de Chile 18 (1), 69-80.

Naranjo, J. A., Moreno, H., Emparan, C., Murphy, M., 1993. Volcanismo explosivo reciente en la caldera del volcàn Sollipulli, Andes del Sur (39°S). Revista Geológica de Chile 20 (2), 167-191.

Nomade, J., Chapron, E., Desmet, M., Reyss, J.-L., Arnaud, F., Lignier, V., 2005. Reconstructing historical seismicity from lake sediments (Lake Laffrey, Western Alps, France). Terra Nova 17, 350-357.

Parra, O., Campos, H., Steffen, W., Aguero, G., Basualto, S., Avilés, D., Vighi, M., 1993. Estudios limnologicos de log lagos Icalma y Galletue: lagos de origen del rio Biobio (Chile central). In: Faranda, F., Parra, O. (Eds), Evaluación de la calidad del agua y ecología del sistema limnético y fluvial del rio Biobio. Monografias Cientificas 12, Concepcion, 161-188.

Rothé, J.-P., 1961. Les séismes du Chili (21 mai - 22 juin 1960). Revue pour l'étude des calamités 37, 3-17.

Schnellmann, M., Anselmetti, F. S., Giardini, D., McKenzie, J. A., Ward, S. N., 2002. Prehistoric earthquake history revealed by lacustrine slump deposits. Geology 30 (12), 1131-1134.

Shiki, T., 1996. Reading of the trigger records of sedimentary events – a problem for future studies. Sedimentary Geology 104, 249-255.

Shiki, T., Kumon, F., Inouchi, Y., Kontani, Y., Sakamoto, T., Tateishi, M., Matsubara, H., Fukuyama, K., 2000. Sedimentary features of the seismo-turbidites, Lake Biwa, Japan. Sedimentary Geology 135, 37-50.

Siegenthaler, C., Finger, W., Kelts, K., Wang, S., 1987. Earthquake and seiche deposits in Lake Lucerne, Switzerland. Eclogae Geologicae Helvetiae 80 (1), 241-260.

Silgado, E., 1985. Terremotos destructivos en América del Sur 1530-1894. CERESIS, Lima, Peru.

St-Onge, G., Mulder, T., Piper, D. J. W., Hillaire-Marcel, C., Stoner, J. S., 2004. Earthquake and flood-induced turbidites in the Saguenay Fjord (Québec): a Holocene paleoseismicity record. Quaternary Science Reviews 23 (3-4), 283-294.

Stuiver M., Reimer P.J., Bard E., Beck J.W., Burr G.S., Hughen K.A., Kromer B., McCormac G., van der Plicht J., Spurk M., 1998. Intcal98 radiocarbon age calibration, 24,000-0 cal BP. Radiocarbon 40 (3), 1041-1083.

Sturm, M., Matter, A., 1978. Turbidites and varves in Lake Brienz (Switzerland): deposition of clastic detritus by density currents. In: Matter, A., Tucker, M. E. (Eds), Modern and ancient lake sediments. Special Publication International Association of Sedimentologists, Oxford, 147-168.

Sturm, M., Siegenthaler, C. Pickrill, R. A., 1995. Turbidites and 'homogenites'. A conceptual model of flood and slide deposits. 5ème congrès de Sédimentologie - ASF. Livre des résumés, 22, Paris, 1p.

Suárez D., Emparan C., 1997. Carta geologica de Chile ; Hoja Curacautin, Regiones de la Araucania y del Biobio. Servicio nacional de geologia y mineria de Chile.

Tazieff, H., 1960. Interprétation des glissements de terrain accompagnant le grand séisme du Chili. Bulletin de la Société belge de Géologie 119, 374-384.

Tazieff, H., 1962. Quelques observations sur la crise séismo-volcanique de mai 1960 au Chili central. Bulletin of Volcanology 24, 83-86.

van Rensbergen, P., De Batist, M., Beck, C., Chapron, E., 1999. High-resolution seismic stratigraphy of glacial to interglacial fill of a deep glacigenic lake: Lake Le Bourget, Northwestern Alps, France. Sedimentary Geology 128, 99-129.

Veyl, C., 1961. Los sismos y las erupciones de mayo de 1960 en el sur de Chile. Boletín Sociedad Chilena de Química 11 (1-2), 20-32.

White, J. D. L., Manville, V., Wilson, C. J. N., Houghton, B. F., Riggs, N. R., Ort, M., 2001. Settling and deposition of AD 181 Taupo pumice in lacustrine and associated environments. Special Publication International Association of Sedimentologists 30, 141-150.

Coring site	Depth	Laboratory n°	Dated material	^{14}C age ± 1σ (yr BP)	Calibrated ages with 2 σ error range (cal. yr. BP)
ICA-I	96.5 cm	Poz-7659	Bulk sediment	2195 ± 35	2110 – 2330 (95.4%)
ICA-I	131.5 cm	Poz-5927	Bulk sediment	3800 ± 35	4080 – 4300 (93.3%)
ICA-I	448 cm	Poz-1407	Wood	4255 ± 35	4650 – 4870 (95.4%)
ICA-I	694.5 cm	Poz-1426	Charcoal	6520 ± 45	7310 – 7560 (95.4%)
ICA-II	104 cm	Poz-7656	Bulk sediment	2140 ± 30	2000 – 2310 (95.4%)
ICA-II	140 cm	Poz-1411	Wood	2450 ± 35	2350 – 2720 (95.4%)
ICA-II	236.5 cm	Poz-1436	Wood	2315 ± 30	2180 – 2360 (95.4%)
ICA-II	352.7 cm	Poz-2203	Bulk sediment	3325 ± 35	3460 – 3640 (95.4%)
ICA-II	508 cm	Poz-7657	Bulk sediment	3410 ± 35	3550 – 3830 (95.4%)
ICA-II	720 cm	Poz-1414	Bulk sediment	6640 ± 50	7430 – 7590 (95.4%)

Table 1 - AMS radiocarbon dates obtained for ICA-I and ICA-II long cores. The range of calibrated ages has been calculated with OxCal 3.9 (Bronk Ramsey, 2001) using atmospheric data of Stuiver et al. (1998).

Figure captions

Figure 1 - Location of the Chilean Lake District in south-central Chile (left) and detailed map of the lakes in their highly active geodynamic setting (right). Epicentres of historical earthquakes with a magnitude > 7 are indicated by a star and labelled with the year of occurrence (Lorca and Recabarren, 1997). LOF: Liquiñe-Ofqui fault and BAF: Biobío-Aluminé fault.

Figure 2 - Position of the coring sites (ICA-I and ICA-II) and location of the seismic profiles shown in this paper (figs. 10 and 11) on the bathymetric map of Parra et al. (1993). Contours are in meters. Note the presence of deeply scoured canyons at the NW flank of the lake watershed.

Figure 3 – Lithology and age-depth models of ICA-I and ICA-II long and short cores. For the short cores, the age-depth models are based on the mean sedimentation rates calculated from ^{210}Pb concentrations (CFCS decay model – Arnaud et al., in press), taking into account the instantaneous deposition of the sedimentary events. The age of the thickest event deposit of each short core has then been calculated by extrapolation of the ^{210}Pb age-depth model (ages labelled ^{210}Pb) and by interpolation of the first radiocarbon date with the top of the core, assuming constant sedimentation rates in-between (ages labelled ^{14}C). For the long cores, the age-depth models are based on 10 AMS radiocarbon dates (table 1) and on a tephrochronological marker previously radiocarbon dated (Alpehue pumice – Naranjo et al. (1993); De Vleeschouwer et al. (2005)). Except for the Alpehue pumice, tephras have been considered as part of the continuous background sedimentation. Grey-shaded bars indicate the presence of seismites. High sedimentation rates above the Alpehue pumice are due to the occurrence of numerous sedimentary events and tephra layers between 3000 and 2200 cal. yr. BP. For details, see table 1 and chapter 7.

Figure 4 – Results obtained on ICA-I long core. (1) grain-size: content in sand (> 63 µm), silt (2-63 µm) and clay (< 2 µm); (2) magnetic susceptibility (9-points running average) and (3) bulk mineralogy with a star indicating the presence of crystallised clay minerals. Four types of event deposits have been described: slump (S), turbidite (T), homogenite (H) and chaotic deposit (C) (see text) and a total of 12 event deposits have been recognized in ICA-I long core: S: 39 – 43 cm; T: 170.5 – 182.5 cm; 460 – 464.8 cm; 469 – 480 cm; 526.5 – 532 cm; 532 – 536 cm; H: 100.3 – 155.5 cm; 640 – 674.7 cm; C: 210.5 – 232.5 cm; 274 – 308.5 cm; 314.3 – 326.8 cm; 331.8 – 367.8 cm. Their cumulative thickness reaches 236.2 cm, i.e. 30% of the length of ICA-I core. T_1 turbidite as well as H_1 and H_2 homogenites are highlighted and their textural characteristics are detailed in figures 6 and 9.

Figure 5 – Results obtained on ICA-II long core. (1) grain-size: content in sand (> 63 µm), silt (2-63 µm) and clay (< 2 µm); (2) magnetic susceptibility (9-points running average) and (3) bulk mineralogy with a star indicating the presence of crystallised clay minerals. Four types of event deposits have been described: slump (S), turbidite (T), homogenite (H) and chaotic deposit (C) (see text) and a total of 10 event deposits have been recognized in ICA-II long core: S: 38 – 43 cm; T: 376 – 384 cm; 406 – 422 cm; 422 – 445 cm; 460 – 478.5 cm; 487 – 495 cm; 717.5 – 734 cm; H : 107.5 – 313 cm; C : 734.15 – 773.15 cm; 789.65 – 804.15 cm. Their cumulative thickness reaches 354 cm, i.e. 43 % of ICA-II long core sediments. H_0 homogenite and T_2 turbidite are highlighted and their textural characteristics are detailed in figures 7, 8 and 9.

Figure 6 - Grain-size parameters and magnetic susceptibility results of H_1 and H_2 homogenites (ICA-I long core, see Fig 4).

Figure 7 - Grain-size parameters and magnetic susceptibility results of H_0 homogenite (ICA-II long core). The three theoretical units of homogenites are clearly distinguished (from base to top: 1-coarse and poorly sorted base, 2-homogeneous unit and 3-thin layer of clayey sediment).

Figure 8 – Textural characterization of H_0 homogenite: sorting versus skewness diagram. The 3 typical units of homogenites defined in figure 7 are clearly identifiable.

Figure 9 - Grain-size parameters and magnetic susceptibility results of T_1 and T_2 turbidites. The mean grain-size profiles show typical fining upward trends. When plotted in a sorting-skewness diagram, the data show a gradual evolution towards better sorting values (compare to fig. 8).

Figure 10 - High resolution (3.5 kHz) seismic cross-section of ICA-I coring site (ical73). The core ICA-I has been projected using a p-wave velocity in the sediment of 1450 m/s. MFD = mass flow deposit. For location, see figure 2. Homogenites H_1 and H_2 are identified by light reflections.

Figure 11 - High resolution (3.5 KHz) seismic cross-section of ICA-II coring site (ical88). The core ICA-II has been projected using a p-wave velocity in the sediment of 1450 m/s. For location, see figure 2. The two thickest units of the homogenite H_0 are identified: its coarse base H_{0b} and the homogenous unit H_{0h}, identified as a light reflection.

Figure 12 - Isopaque map of the two main units of H_0 homogenite: coarse and disturbed base (H_{0b}) and homogeneous unit (H_{0h}). The arrows indicate the main mass-flow directions. At site ICA-I the two units of H_0 homogenite are too thin to be accurately mapped. Approximately, 3ms TWT = 2.4m and 1.25ms TWT = 1m.

Figure 13 – Thickness of the sedimentary events identified in ICA-I and ICA-II cores, plotted against their calculated age. The nature of the sedimentary events is indicated: (S) slump deposit, (H) homogenite, (T) turbidite, (C) chaotic deposit. Note the change of scale for the ICA-II thickness axis. The volcano represents the Alpehue eruption of Sollipulli volcano in 3000 cal. yr. BP.

Figure 14 – Sedimentary processes occurring during the deposition of H_0 and H_1 homogenites. See text for details. Illustration inspired from the figure 11 of Shiki et al. (2000).

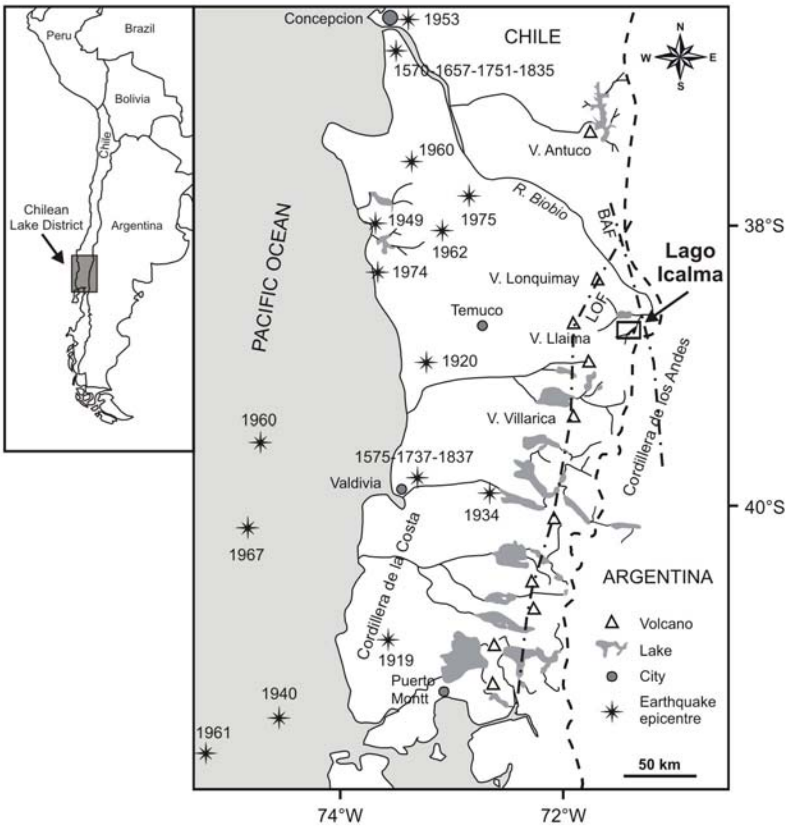

Figure 1 - Bertrand et al.

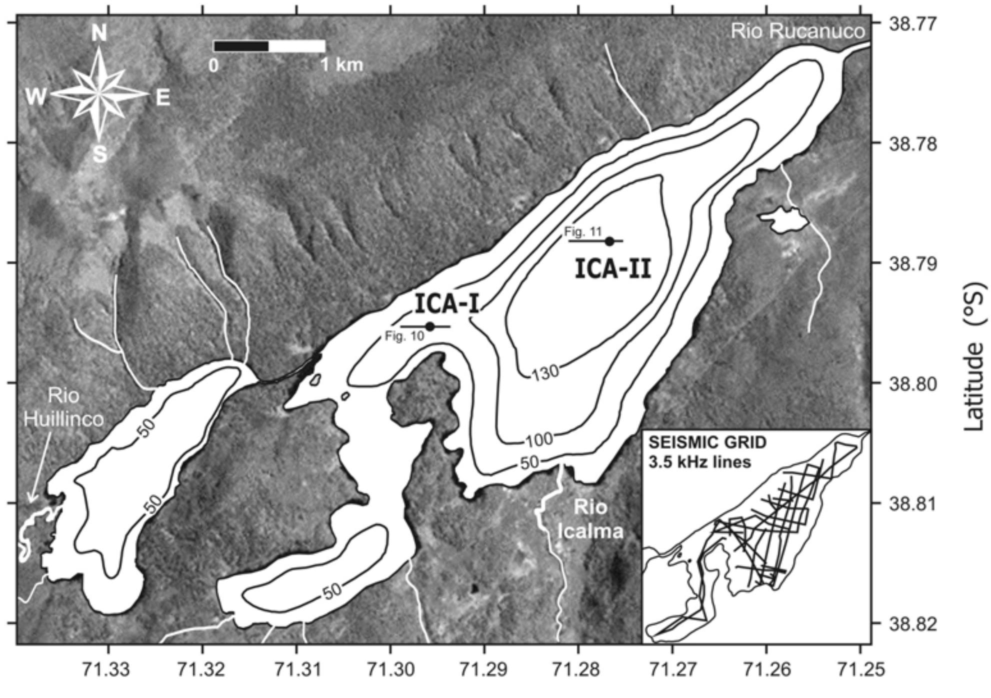

Figure 2 - Bertrand et al.

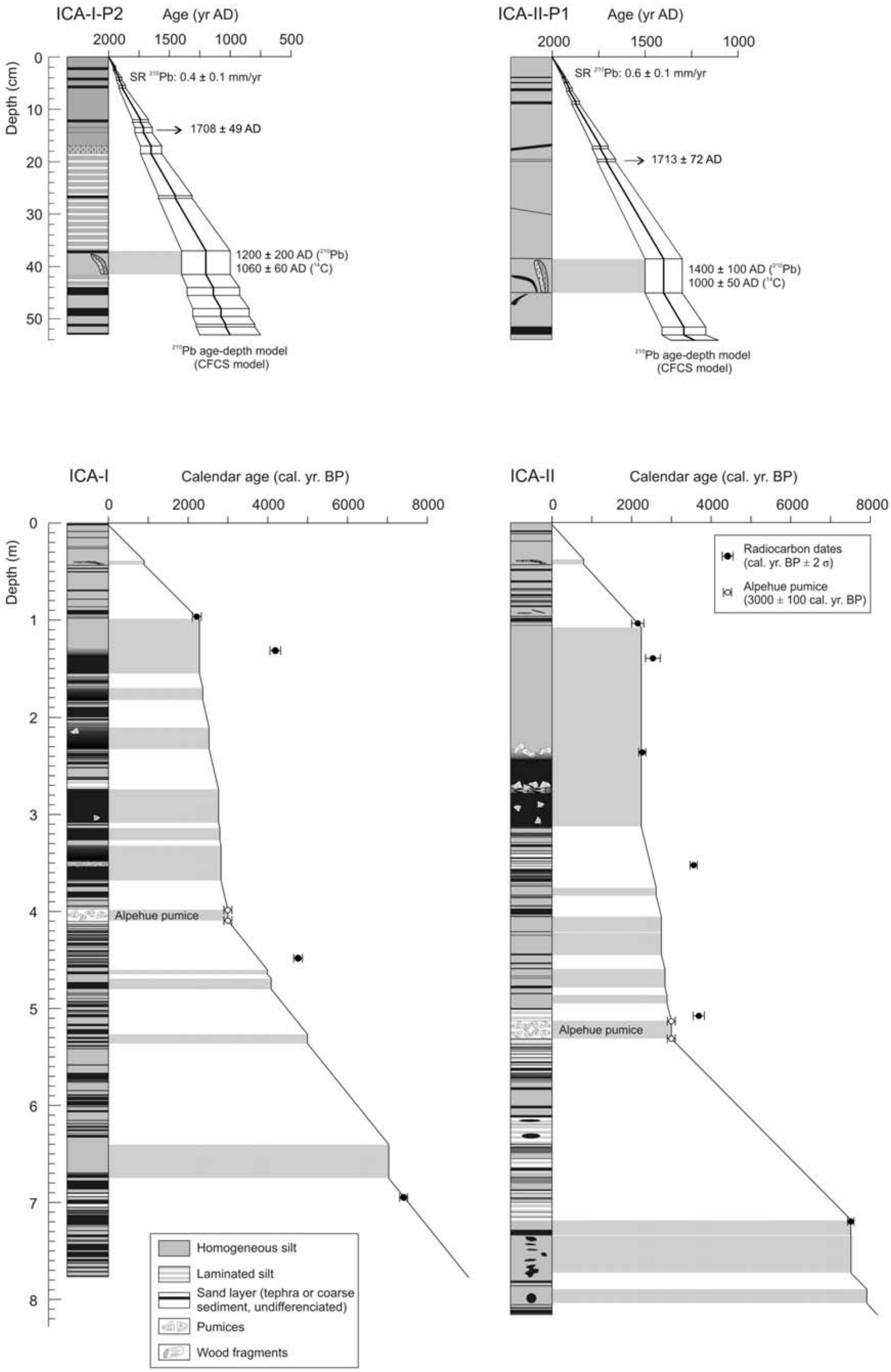

Figure 3 - Bertrand et al

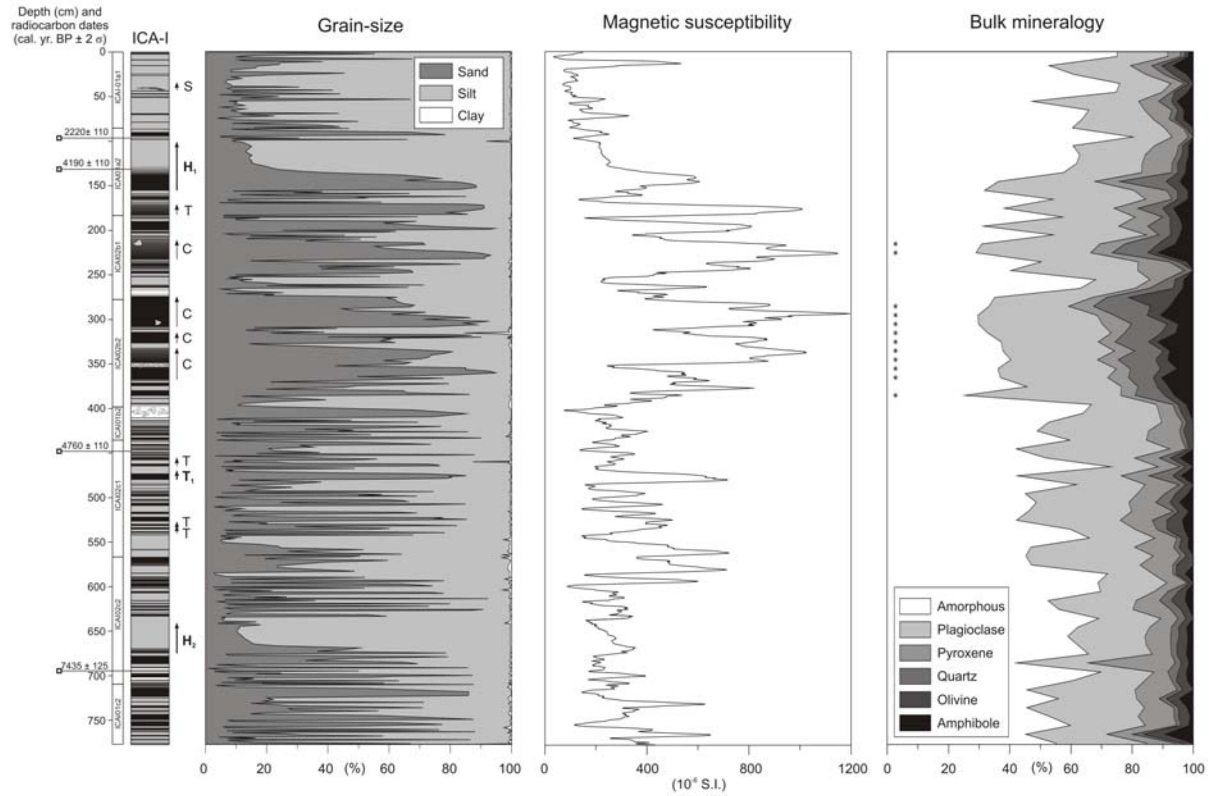

Figure 4 – Bertrand et al.

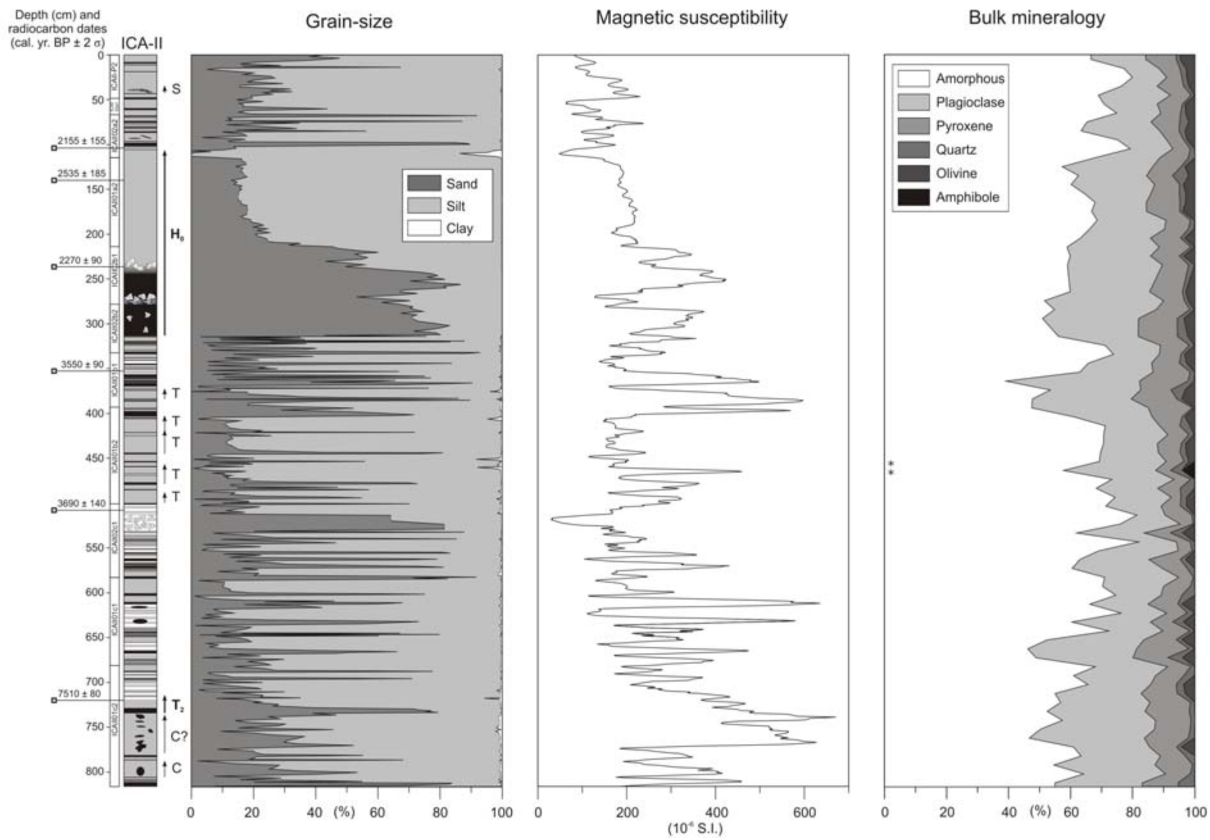

Figure 5 – Bertrand et al

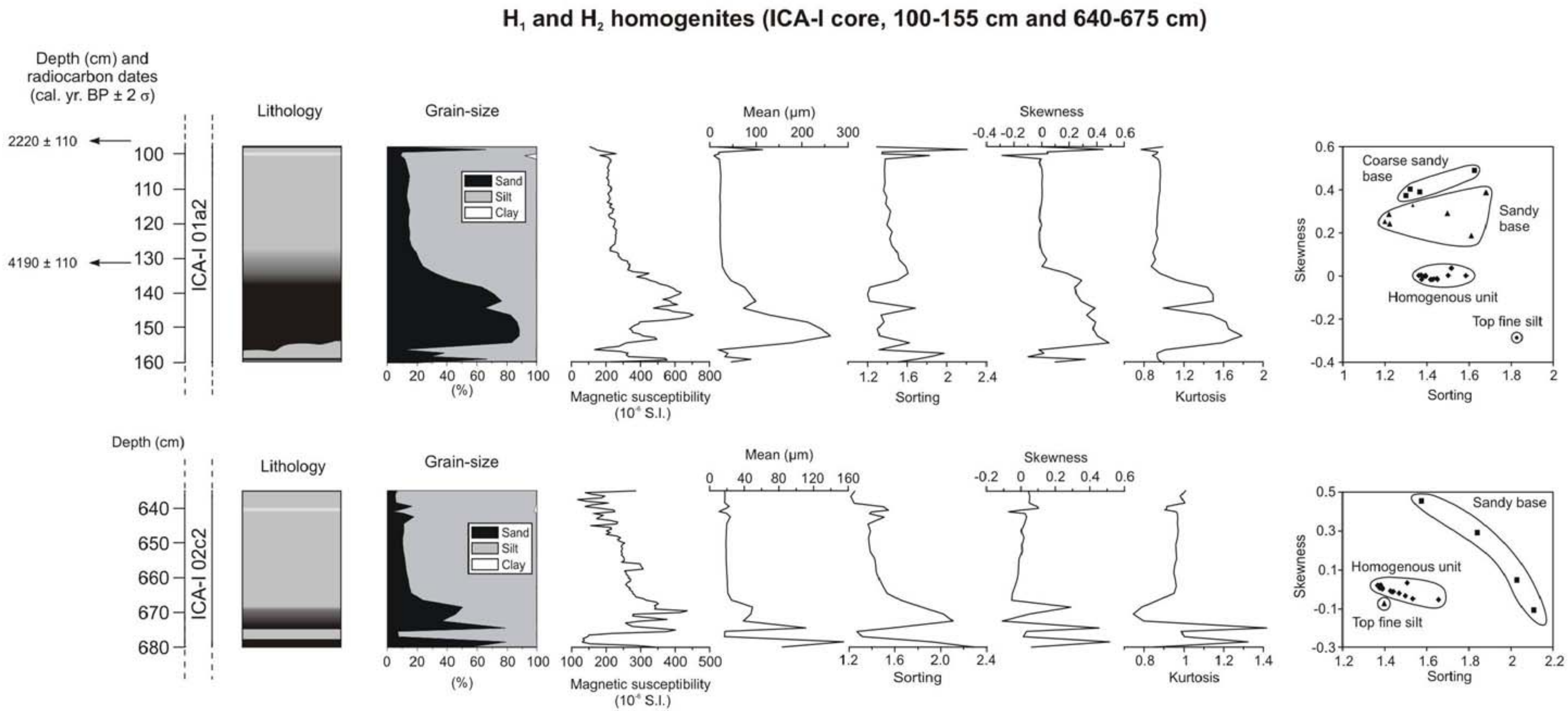

Figure 6 – Bertrand et al.

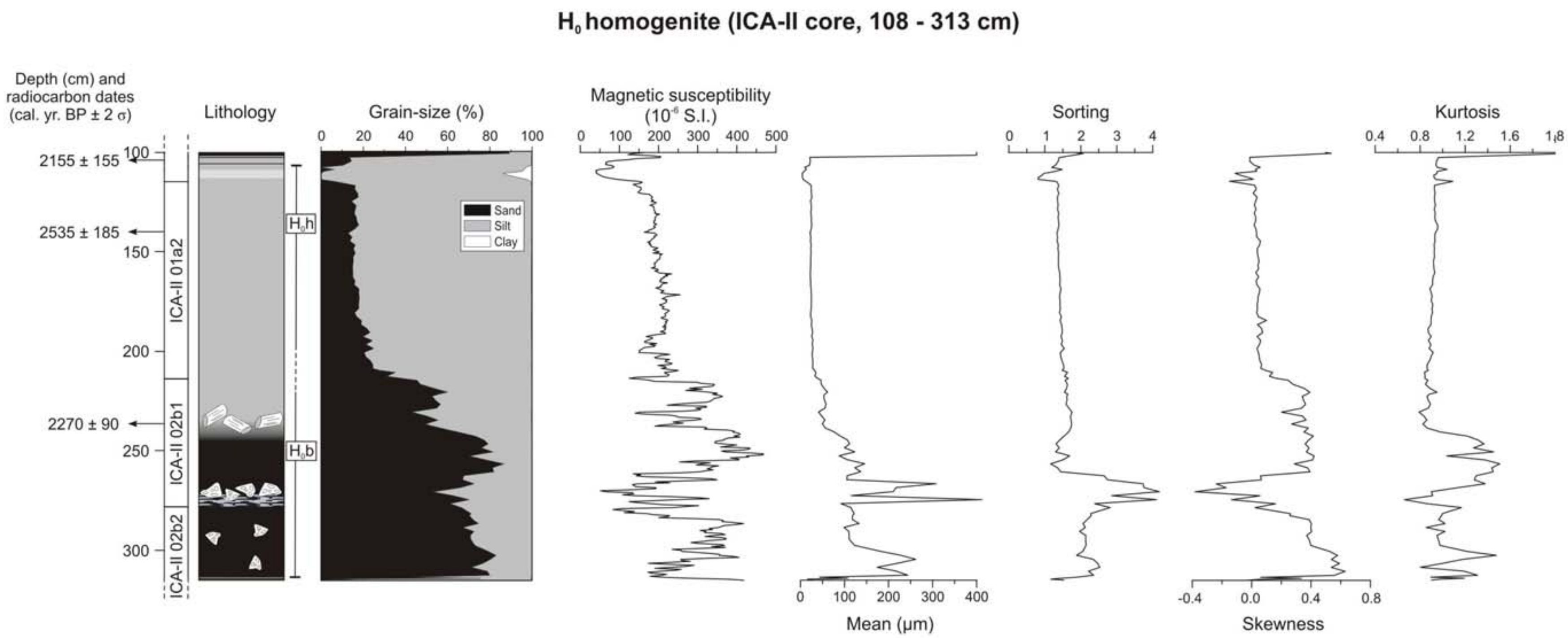

Figure 7 – Bertrand et al.

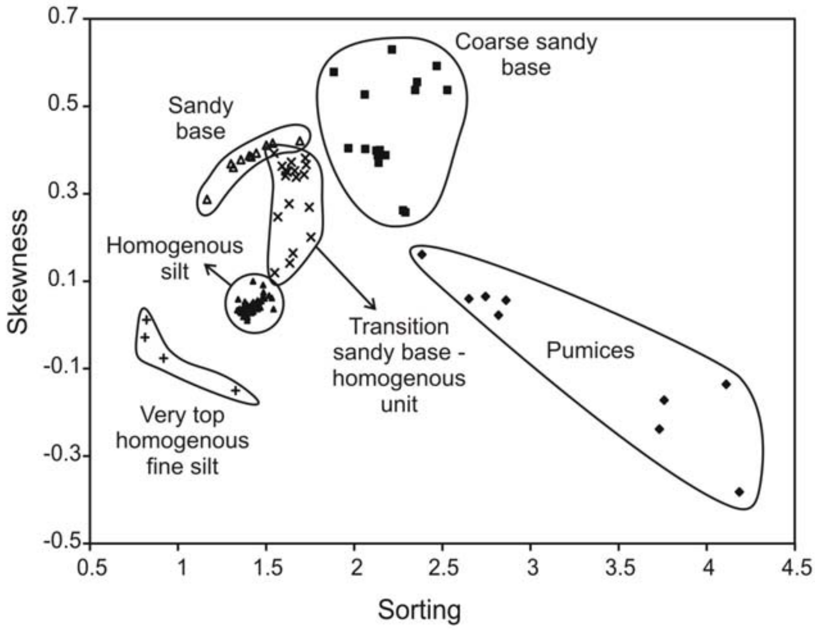

Figure 8 – Bertrand et al.

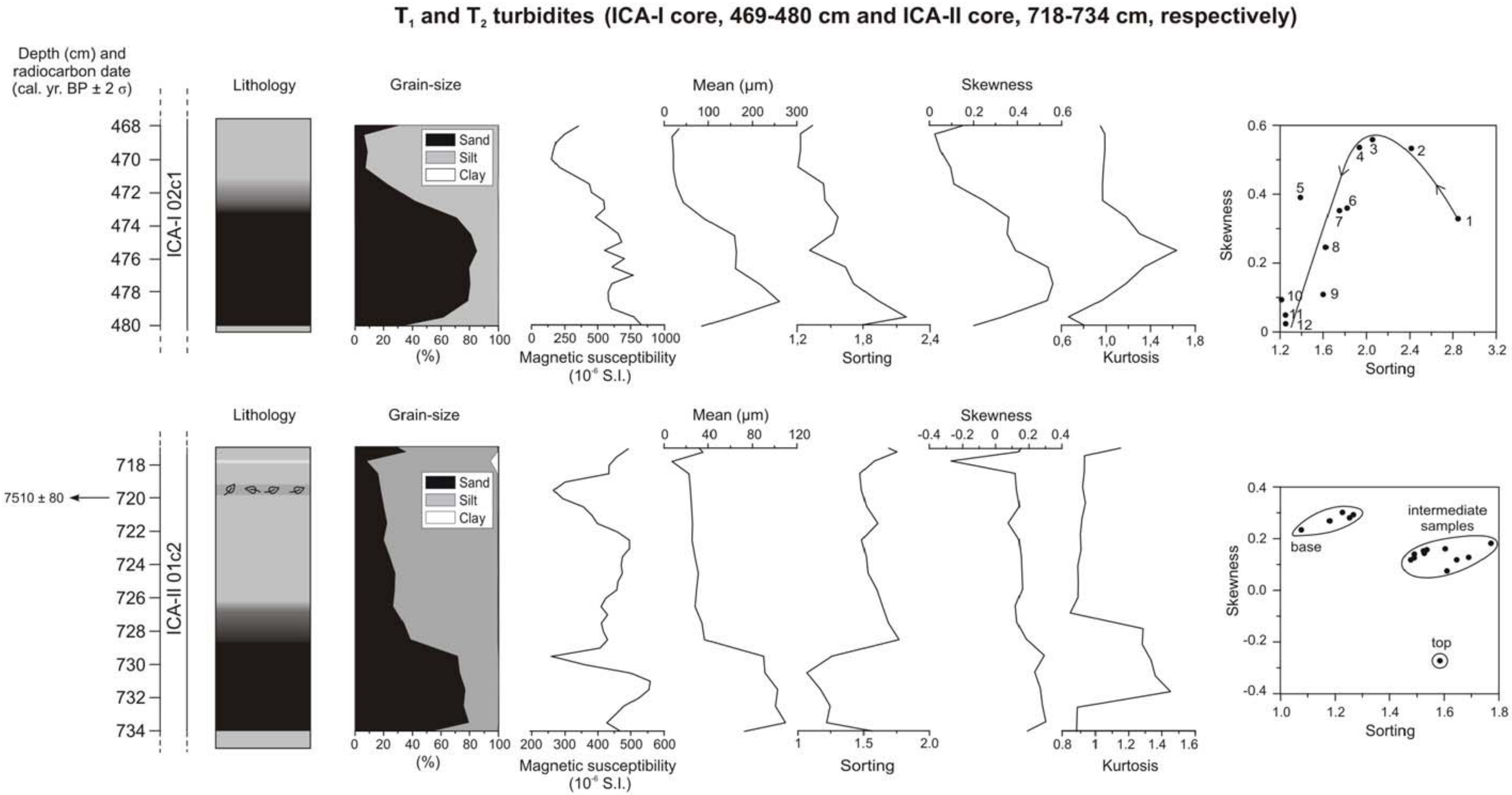

Figure 9 – Bertrand et al.

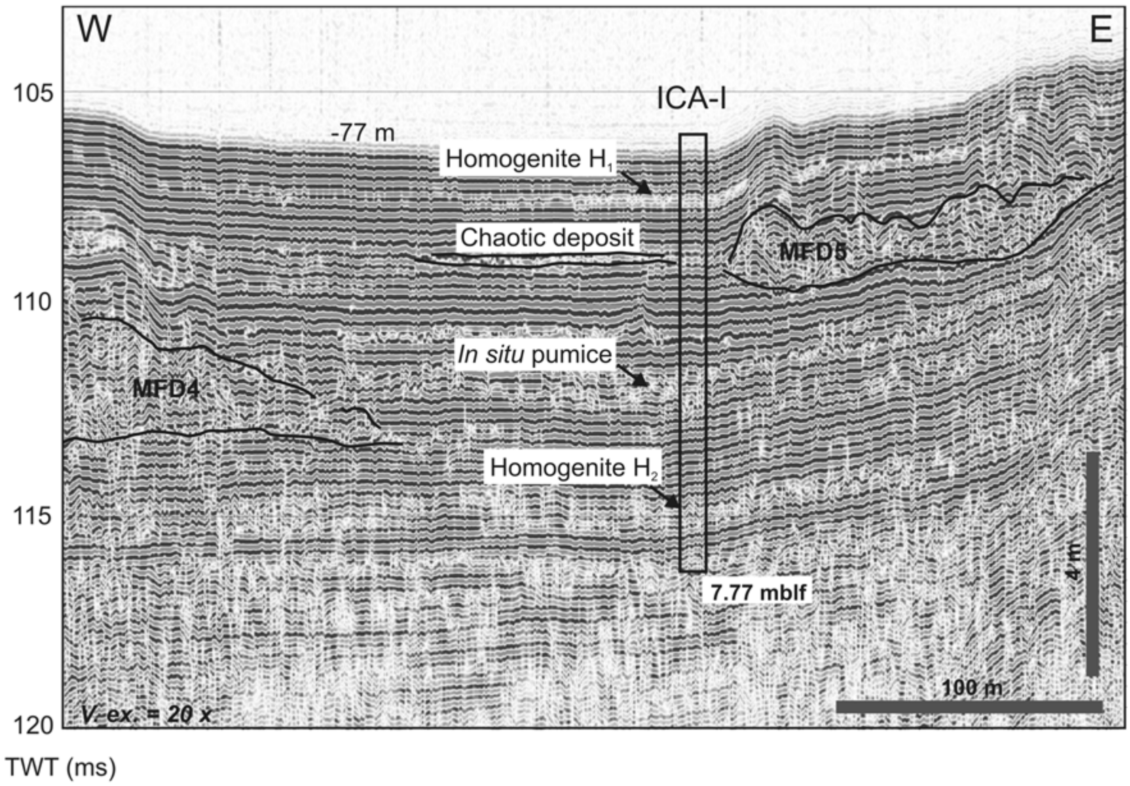

Figure 10 – Bertrand et al.

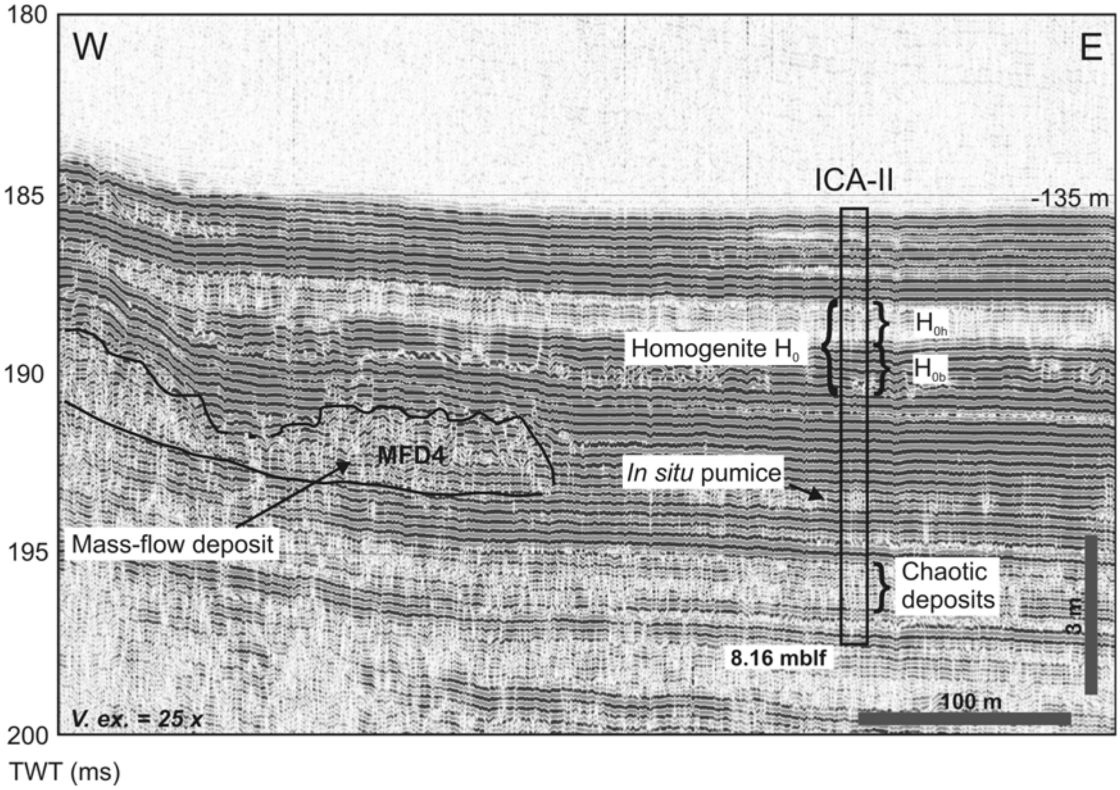

Figure 11 – Bertrand et al.

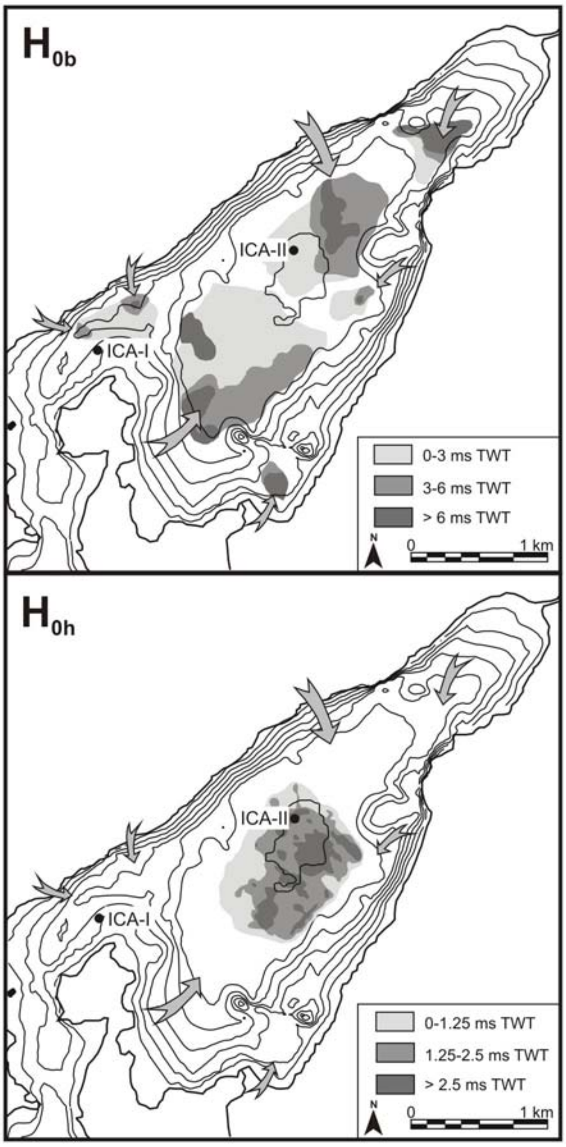

Figure 12 – Bertrand et al.

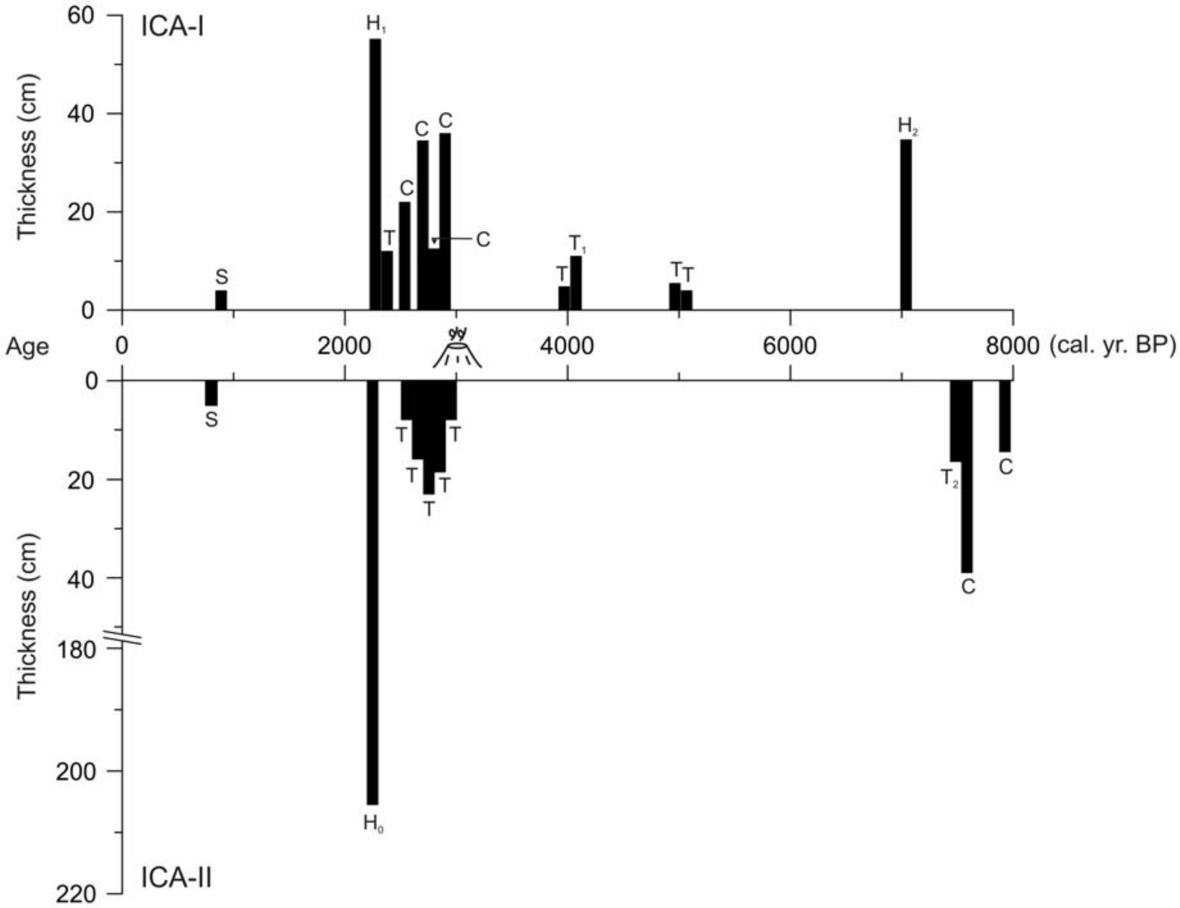

Figure 13 – Bertrand et al.

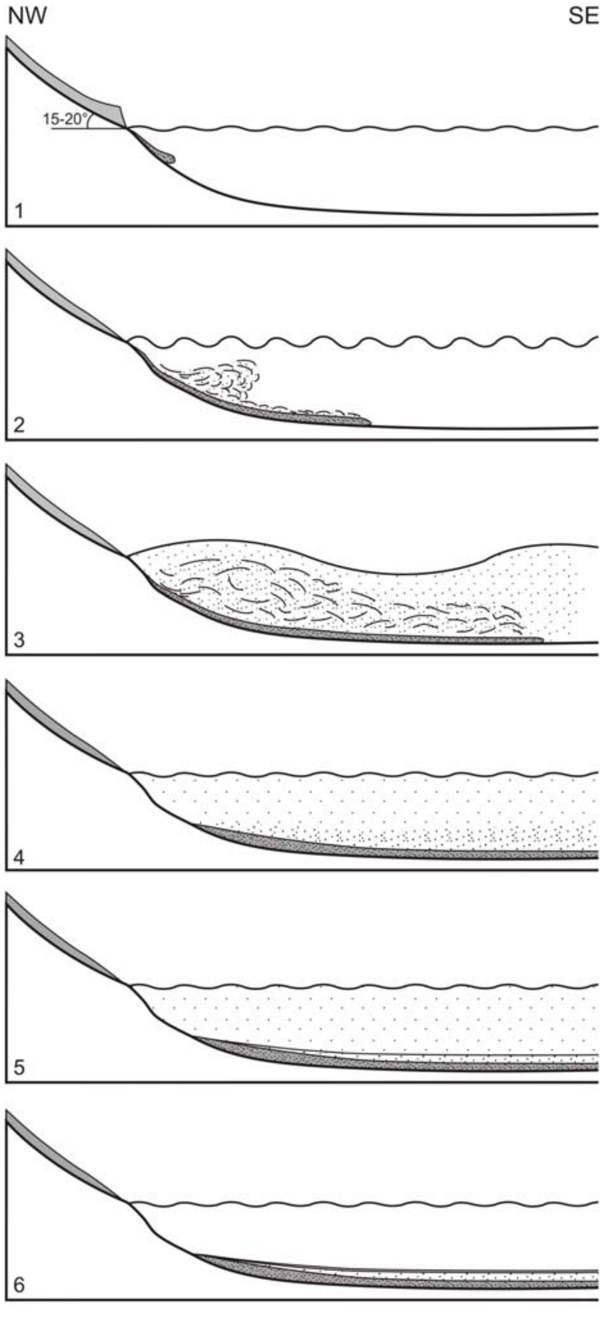

Figure 14 – Bertrand et al.